

Conditional Random Fields as Recurrent Neural Networks for 3D Medical Imaging Segmentation

Miguel Monteiro*¹, Mário A. T. Figueiredo^{2,3}, and
Arlindo L. Oliveira^{1,2}

¹INESC-ID

²Instituto Superior Técnico, Universidade de Lisboa

³Instituto de Telecomunicações

Abstract

The Conditional Random Field as a Recurrent Neural Network layer is a recently proposed algorithm meant to be placed on top of an existing Fully-Convolutional Neural Network to improve the quality of semantic segmentation. In this paper, we test whether this algorithm, which was shown to improve semantic segmentation for 2D RGB images, is able to improve segmentation quality for 3D multi-modal medical images. We developed an implementation of the algorithm which works for any number of spatial dimensions, input/output image channels, and reference image channels. As far as we know this is the first publicly available implementation of this sort. We tested the algorithm with two distinct 3D medical imaging datasets, we concluded that the performance differences observed were not statistically significant. Finally, in the discussion section of the paper, we go into the reasons as to why this technique transfers poorly from natural images to medical images.

1 Introduction

Using a fully-connected Conditional Random Field (CRF) [6] in conjunction with a Fully-Convolutional Neural Network (FCNN) [8] is the state-of-the-art type of approach for semantic segmentation of two-dimensional natural images [3].

The core idea behind this approach is that the FCNN will serve as a feature extractor that produces a coarse segmentation which is later refined by the CRF. The CRF takes as input the segmentation produced by the network as well as the original input image. Unlike a convolution layer which employs local filters, the CRF looks at every possible pair of pixels in the image, also known as a

*Corresponding author: mab.mtr@gmail.com

clique. The CRF is a graphical model where every clique is defined not only by the spatial distance between pixels but also by their distance in colour space. This allows the CRF to produce a segmentation with much sharper edges when compared with only using a FCNN.

This means that the receptive field of a CRF is the entire image.

Graphical models such as the fully-connected CRF have also been extensively used in 3D medical imaging segmentation with good results [2, 4, 5, 10, 12]. One of the issues with applying a fully-connected CRF to 3D images is the fact that the third dimension introduces exponentially more pairs of hyper-voxels in the graph, also known as cliques. For example, if a 2D square image with *width* = N will have N^2 cliques in the graph, a 3D image with the same width will have N^3 cliques in the graph. This makes these models more expensive and likely justifies why they are not as widespread in 3D medical images as in 2D images.

Another issue with using a CRF to improve the quality of a segmentation is that the CRF has to be trained separately after the base classifier has been trained. Because of this, in [13] the authors propose writing the CRF mean-field approximation described in [6] as an Recurrent Neural Network (RNN) which can be placed on top of Convolutional Neural Network (CNN) and train the whole system end-to-end.

As far as we know, this system has not been tested for three-dimensional medical images. As a result, we set out to test if this algorithm could be successfully applied in this domain.

2 Methods

2.1 Theoretical background.

In this section we present a summary of theoretical background of a fully-connected CRF [6].

Consider an n -dimensional image with N hyper-voxels (pixels, voxels, 4D-voxels, etc...) on which we wish to perform semantic segmentation, *i.e.* to assign a label to every hyper-voxels. We define X_j and I_j to be the label and colour value of hyper-voxel j , respectively.

Consider a random field \mathbf{X} defined over a set of variables $\{X_1, X_2, \dots, X_N\}$ each taking a value from a set of labels $\mathcal{L} = \{l_1, l_2, \dots, l_k\}$. Consider another random field \mathbf{I} defined over the variables $\{I_1, I_2, \dots, I_N\}$ where the domain of each variable is the possible colour values of a hyper-voxel in the image.

A Conditional Random Field (\mathbf{I}, \mathbf{X}) is characterized by a Gibbs distribution:

$$P(\mathbf{X}|\mathbf{I}) = \frac{1}{Z(\mathbf{I})} \exp \left(- \sum_{c \in \mathcal{C}_{\mathcal{G}}} \phi_c(\mathbf{X}_c|\mathbf{I}) \right), \quad (1)$$

where \mathcal{G} is a graph on \mathbf{X} and each clique c in the set of cliques $\mathcal{C}_{\mathcal{G}}$ induces a potential ϕ_c . The Gibbs energy of labelling $\mathbf{x} \in \mathcal{L}^N$ is $E(\mathbf{x}|\mathbf{I}) = \sum_{c \in \mathcal{C}_{\mathcal{G}}} \phi_c(\mathbf{X}_c|\mathbf{I})$

and the maximum a posteriori (MAP) labelling of the random field is $\mathbf{x}^* = \arg \max_{\mathbf{x} \in \mathcal{L}^N} P(\mathbf{X}|\mathbf{I})$. $Z(\mathbf{I})$ is a normalization constant that ensures $P(\mathbf{X}|\mathbf{I})$ is a valid probability distribution. For notational convenience the conditioning will be omitted from now on, we define $\psi_c(\mathbf{x}_c)$ to denote $\phi_c(\mathbf{x}_c|\mathbf{I})$.

The Gibbs energy of the fully-connected pairwise CRF is the set of all unary and pairwise potentials:

$$E(x) = \sum_i \psi_u(x_i) + \sum_{i < j} \psi_p(x_i, x_j), \quad (2)$$

where i and j range from 1 to N . The unary potential $\psi_u(x_i)$ is computed independently for each hyper-voxel by a classifier, *i.e.* the choice of label for one hyper-voxel does have a direct impact on the labels of other hyper-voxels.

The pairwise potentials are given by:

$$\psi_p(x_i, x_j) = \mu(x_i, x_j) \underbrace{\sum_{m=1}^K w^{(m)} k^{(m)}(\mathbf{f}_i, \mathbf{f}_j)}_{k(\mathbf{f}_i, \mathbf{f}_j)}, \quad (3)$$

where $k^{(m)}$ is a Gaussian kernel applied to arbitrary feature vectors \mathbf{f}_i and \mathbf{f}_j , $w^{(m)}$ is linear combination of trainable weights and μ is a compatibility function between labels.

The feature vectors \mathbf{f}_i and \mathbf{f}_j can be constructed from any feature space regarding the image. However, in this setting, they are chosen to take into account positions p_i and p_j , and the colour values I_i and I_j of the hyper-voxels in the image:

$$k(\mathbf{f}_i, \mathbf{f}_j) = \underbrace{w^{(1)} \exp\left(-\frac{|p_i - p_j|^2}{2\theta_\alpha^2} - \frac{|I_i - I_j|^2}{2\theta_\beta^2}\right)}_{\text{appearance kernel}} + \underbrace{w^{(2)} \exp\left(-\frac{|p_i - p_j|^2}{2\theta_\gamma^2}\right)}_{\text{smoothness kernel}}. \quad (4)$$

The parameters θ_α , θ_β and θ_γ are hyper-parameters that control the importance of the hyper-voxel difference in a specific feature space. This choice of $k(\mathbf{f}_i, \mathbf{f}_j)$ includes both an appearance kernel (aka bilateral kernel), which penalizes different labels for hyper-voxels that are close in space and color value, and a smoothness kernel (aka Gaussian kernel) which penalizes different labels for hyper-voxels close only in space.

In our case, the compatibility function, μ , is a k by k matrix learnt from the data. It has zeros along its diagonal and trainable weights elsewhere in order for the model to be able to penalize different pairs of labels differently. For instance, in brain tumour segmentation we might want to penalize assigning the background class to the tumour's core more than assigning the oedema class to the tumour's core.

Since the direct computation of $P(\mathbf{X})$ is intractable we use the mean field approximation to compute the distribution $Q(\mathbf{X})$ that minimizes the KL-divergence

$\mathbf{D}(Q||P)$, where Q can be written as a product of independent marginals, $Q(\mathbf{X}) = \prod_i Q_i(X_i)$.

Minimizing the KL-divergence yields the following iterative update equation:

$$Q_i(x_i = l) = \frac{1}{Z_i} \exp \left(-\psi_u(x_i) - \sum_{l' \in \mathcal{L}} \mu(l, l') \sum_{m=1}^K w^{(m)} \sum_{i \neq j} k^{(m)}(\mathbf{f}_i, \mathbf{f}_j) Q_j(l') \right), \quad (5)$$

which leads to the inference algorithm detailed in Algorithm 1.

Algorithm 1: CRF mean field approximation.

| | |
|---|-------------------------|
| $Q_i(x_i) = \frac{1}{Z_i} \exp\{-\phi_u(x_i)\};$ | Initialize Q |
| while <i>not converged</i> do | |
| $\tilde{Q}_i^{(m)}(l) \leftarrow \sum_{i \neq j} k^{(m)}(\mathbf{f}_i, \mathbf{f}_j) Q_j(l)$ for all m ; | Message passing |
| $\hat{Q}_i(x_i) \leftarrow \sum_{l \in \mathcal{L}} \mu^{(m)}(x_i, l) \sum_m w^{(m)} \tilde{Q}_i^{(m)}(l);$ | Compatibility transform |
| $Q_i(x_i) \leftarrow \exp\{-\psi(x_i) - \hat{Q}_i(x_i)\};$ | Local update |
| normalize $\hat{Q}_i(x_i)$ | |
| end | |

The only step in Algorithm 1 that is not straightforward is the message passing step from every X_i to X_j . For our choice of kernels, this step involves applying a bilateral and a Gaussian filter to Q . A brute force implementation has a time complexity of $\mathcal{O}(N^2)$, therefore, we use the permutohedral lattice to approximate high-dimensional filtering [1] which has linear time complexity with N (even though it has quadratic time complexity with the number of dimensions of the position vectors).

The key insight of the CRF as RNN paper [13] is that this inference algorithm can be written as a sequence of steps which can propagate gradient backwards like a RNN. This can be easily implemented in an existing deep learning framework. The authors called this new layer a CRF as RNN layer which can be placed on top of existing CNN architectures to improve the quality of semantic segmentation. The main advantage of this layer is the ability to train a model which includes a CRF end-to-end with gradient descent methods.

2.2 Implementation

The previously proposed system was designed and implemented for 2D RGB images. In our work, we adapted the algorithm to work with n-dimensional images and with any number of channels.

From a conceptual stand-point extending this algorithm to the general case is straightforward. However, the implementation details are a bit more complicated and hence are the core contribution of this work. Most of the steps in the inference algorithm can be easily written using existing operations in popular deep learning frameworks. Unfortunately, the message passing step which

involves high-dimensional filtering cannot be easily implemented using existing operations.

Both public implementations of the fully-connected CRF and CRF as RNN algorithms are based on the permutohedral lattice algorithm [1] and the code provided in that paper. The permutohedral lattice is a fast approximation of high dimensional filters which can be used for Gaussian and bilateral filtering. The available implementation of the permutohedral lattice was designed for 2D RGB images and only used CPU kernels ¹.

The brunt of this work was re-implementing the permutohedral lattice so that:

- The implementation supported any number of spatial dimensions, input channels/output channels (class labels from the perspective of the CRF) and reference image channels.
- The implementation contained not only a CPU C++ kernel but also as a C++/CUDA kernel for fast computation in GPU.
- The implementation included a TensorFlow Op wrapper so that it could be easily used in Python and incorporated in any TensorFlow graph.

Our code for the permutohedral lattice (both CPU and GPU) implemented as a TensorFlow operation is available at https://github.com/MiguelMonteiro/permutohedral_lattice. The code for the CRF as RNN algorithm also implemented in TensorFlow and which uses the aforementioned permutohedral lattice is available at <https://github.com/MiguelMonteiro/CRFasRNNLayer>.

3 Experiments

To test whether using the CRF as RNN layer on top of a CNN improved the segmentation quality for 3D medical images, we conducted two experiments.

The aim of these experiments was not to achieve the best possible performance on these tasks, but to compare the performance difference between using and not using the proposed algorithm.

The underlying network architecture used for segmentation was the V-Net architecture [11].

3.1 PROMISE 2012

The PROMISE 2012 dataset [7] is a set of 50 three-dimensional Magnetic Resonance Imaging (MRI) prostate images and the respective expert segmentations of the prostate. The images have different resolutions and a different number of slices, regardless, they all have one channel. In our experiment, we re-sampled the images so that they all had resolution $1 \times 1 \times 2$ millimetres. This resulted in

¹The authors of the permutohedral lattice paper also provided a GPU implementation which proved to be slower than the CPU version due to bugs in the code.

images of size $[x, y, z, c] = [200, 200, 63, 1]$ voxels, where c denotes the channel dimension. An example slice from the PROMISE 2012 dataset along with the respective expert segmentation is shown in Figure 1.

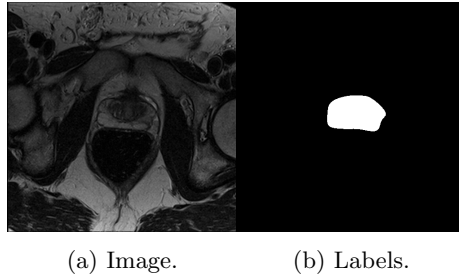


Figure 1: PROMISE 2012 example slice.

Since this is a binary segmentation problem the performance metric used is simply the Dice Coefficient (DC).

Given that there were only 50 labelled images we used 5-fold cross-validation and ran each fold for 200 epochs (8000 steps). The results for this experiment with and without the CRF as RNN layer are presented in Table 1.

Table 1: PROMISE 2012 results

| | Dice Coefficient |
|-------------|-------------------|
| Without CRF | 0.767 ± 0.109 |
| With CRF | 0.780 ± 0.110 |

3.2 BraTS 2015 High-Grade Gliomas

The Multimodal Brain Tumor Segmentation Challenge 2015 (BraTS 2015) [9] training dataset for High-Grade Glioma (HGG) is composed of 220 multimodal MRI images of brain tumors. All of the images have the same resolution $1 \times 1 \times 1$ millimeters and the same size ($[x, y, z] = [240, 240, 155]$ voxels). For each case there exist 4 different images (T1, T1c, T2 and Flair). This results in images of size $[x, y, z, c] = [240, 240, 155, 4]$.

The expert segmentation has 5 distinct labels: background, oedema, enhancing tumour core, non-enhancing tumour core and necrotic tumour core. However, the main performance metrics for this task are the whole tumour DC (includes everything except the background) and the core tumour DC (only includes the enhancing, non-enhancing and necrotic cores). An example slice from the BraTS 2015 dataset along with the respective expert segmentation is shown in Figure 2.

For our experiments, we split the data-set into training and holdout set (85%/15%) which meant that 33 cases were used to measure performance on.

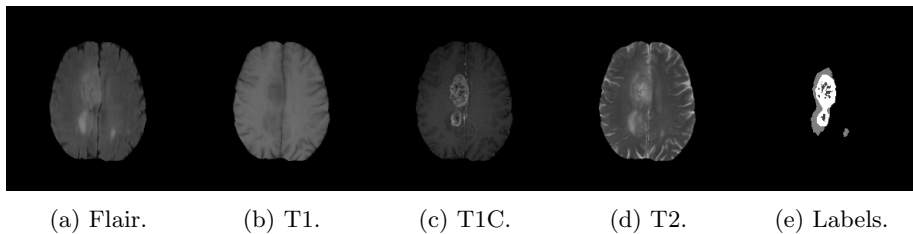


Figure 2: BraTS 2015 HGG example slice.

The network was trained for 100 epochs (18700 steps). The results for this experiment with and without the CRF as RNN layer are presented in Table 2.

Table 2: BraTS 2015 HGG Results

| | Whole Tumor Dice Coefficient | Core Tumor Dice Coefficient |
|-------------|------------------------------|-----------------------------|
| Without CRF | 0.735 ± 0.105 | 0.488 ± 0.244 |
| With CRF | 0.738 ± 0.105 | 0.482 ± 0.257 |

4 Discussion

Looking at close means and large standard deviations presented in Table 1 we can see that it is unlikely that a statistical test will reveal that the small performance increase in using the CRF is statistically significant. In fact, a paired t-test reveals exactly this: the performance difference between using and not using the CRF as RNN is not statistically significant. The same is true for the results of the BraTS 2015 experiment, presented in Table 2.

Hence, we conclude that using the CRF as RNN layer on top of a CNN does not improve the segmentation quality. The fact that this algorithm seemingly works for 2D RGB images [13] but not for 3D MRI medical images can be due to a number of factors. Here we explore some of those factors.

Natural images tend to have much higher contrast and much sharper edges than MRI images. The edges between objects in natural images tend to be much more well defined (e.g. A building against a blue sky) than in MRI images (e.g. the oedema in a brain MRI is a slightly different shade of grey than the healthy region surrounding it). Since MRI images have much less contrast and tend to have blurry edges, the object of interest often fuses with the background slowly and seamlessly. Trained radiologists can use their knowledge of human anatomy and pathology in conjunction with the observed image to infer where the object of interest starts and ends. In contrast, the CRF only has access to differences between hyper-voxels, and these differences are zero or close to zero in low contrast, blurry edge environments. This means that there is much more sensitivity to the parameters θ_α , θ_β and θ_γ . Setting these parameters becomes

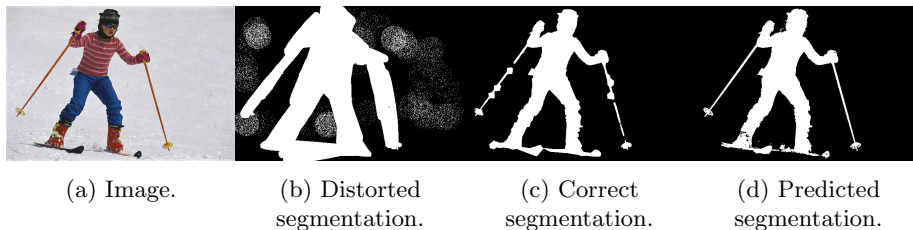


Figure 3: 2D RGB experiment.

very difficult and when taking into account inter-image variability observed during training, there simply isn't a set of θ parameters that works for all (or most of) the images.

Despite having many voxels, 3D medical images have much lower resolution than natural images which compounds the problem of having blurry edges.

The regions of interest to be segmented in medical images tend to be "local". In our experiment, the prostate and brain tumours fit inside the receptive field of the neural network. This may not be the case in natural images where we might, for example, want to segment multiple birds out of the sky. For this reason, it is possible that the FCNN was already able to capture all of the relevant spatial and colour relations in the image and hence the CRF has no room to improve.

One thing the reader might be wondering at this point is whether there was a bug with our implementation. To test this proposition we tested our implementation of the algorithm for 2D RGB images. We took an image and its respective segmentation, we distorted the segmentation to simulate the output of a "bad" CNN. After, we overfitted the CRF as RNN layer by giving it as input the distorted segmentation and minimizing the cross-entropy between the output of the CRF as RNN layer and the correct labels. The results of this experiment are shown in Figure 3. As we can see from Figure 3 the predicted segmentation that is accomplished just by training two scalar weights on filter outputs and running the recurrent inference algorithm gives better results than even the expert provided segmentation (as seen from the skier's baton). This indicates that both the filters and inference algorithm are implemented correctly.

We also performed the same experiment for 3D medical images from the PROMISE 2012 and BraTS 2015 dataset and observed that the CRF as RNN layer was able to remove the greater part of the noise. However, the algorithm was not able to overfit the visual features nearly as well as in the 2D RGB case.

5 Conclusion

In this paper we applied the CRF as RNN layer for semantic segmentation to 3D medical imaging segmentation. As far as we know we provide the first publicly available version of this algorithm that works for any number of spatial

dimensions, input/output channels and reference channels. We tested the CRF as RNN layer on top a FCNN (with a V-Net architecture) on two distinct medical imaging datasets. We concluded that the performance differences observed were not statically significant and we provide a discussion as to why this technique does not transfer well from 2D RGB images to 3D multi-modal medical images.

References

- [1] Andrew Adams, Jongmin Baek, and Myers Abraham Davis. Fast high-dimensional filtering using the permutohedral lattice. In *Computer Graphics Forum*, volume 29, pages 753–762. Wiley Online Library, 2010.
- [2] Jinzheng Cai, Le Lu, Zizhao Zhang, Fuyong Xing, Lin Yang, and Qian Yin. Pancreas segmentation in mri using graph-based decision fusion on convolutional neural networks. In Sebastien Ourselin, Leo Joskowicz, Mert R. Sabuncu, Gozde Unal, and William Wells, editors, *Medical Image Computing and Computer-Assisted Intervention - MICCAI 2016*, pages 442–450, Cham, 2016. Springer International Publishing.
- [3] L. C. Chen, G. Papandreou, I. Kokkinos, K. Murphy, and A. L. Yuille. Deeplab: Semantic image segmentation with deep convolutional nets, atrous convolution, and fully connected crfs. *IEEE Transactions on Pattern Analysis and Machine Intelligence*, 40(4):834–848, April 2018.
- [4] Patrick Ferdinand Christ, Mohamed Ezzeldin A. Elshaer, Florian Ettl, Sunil Tataavarty, Marc Bickel, Patrick Bilic, Markus Rempfler, Marco Armbruster, Felix Hofmann, Melvin D’Anastasi, Wieland H. Sommer, Seyed-Ahmad Ahmadi, and Bjoern H. Menze. Automatic liver and lesion segmentation in ct using cascaded fully convolutional neural networks and 3d conditional random fields. In Sebastien Ourselin, Leo Joskowicz, Mert R. Sabuncu, Gozde Unal, and William Wells, editors, *Medical Image Computing and Computer-Assisted Intervention - MICCAI 2016*, pages 415–423, Cham, 2016. Springer International Publishing.
- [5] Huazhu Fu, Yanwu Xu, Stephen Lin, Damon Wing Kee Wong, and Jiang Liu. Deepvessel: Retinal vessel segmentation via deep learning and conditional random field. In Sebastien Ourselin, Leo Joskowicz, Mert R. Sabuncu, Gozde Unal, and William Wells, editors, *Medical Image Computing and Computer-Assisted Intervention - MICCAI 2016*, pages 132–139, Cham, 2016. Springer International Publishing.
- [6] Philipp Krähenbühl and Vladlen Koltun. Efficient inference in fully connected crfs with gaussian edge potentials. In *Advances in neural information processing systems*, pages 109–117, 2011.
- [7] Geert Litjens, Robert Toth, Wendy van de Ven, Caroline Hoeks, Sjoerd Kerkstra, Bram van Ginneken, Graham Vincent, Gwenael Guillard,

- Neil Birbeck, Jindang Zhang, Robin Strand, Filip Malmberg, Yangming Ou, Christos Davatzikos, Matthias Kirschner, Florian Jung, Jing Yuan, Wu Qiu, Qinquan Gao, Philip “Eddie” Edwards, Bianca Maan, Ferdinand van der Heijden, Soumya Ghose, Jhimli Mitra, Jason Dowling, Dean Barratt, Henkjan Huisman, and Anant Madabhushi. Evaluation of prostate segmentation algorithms for mri: The promise12 challenge. *Medical Image Analysis*, 18(2):359 – 373, 2014.
- [8] Jonathan Long, Evan Shelhamer, and Trevor Darrell. Fully convolutional networks for semantic segmentation. In *Proceedings of the IEEE conference on computer vision and pattern recognition*, pages 3431–3440, 2015.
- [9] Bjoern Menze, Andras Jakab, Stefan Bauer, Jayashree Kalpathy-Cramer, Keyvan Farahani, Justin Kirby, Yuliya Burren, Nicole Porz, Johannes Slotboom, Roland Wiest, Levente Lenczi, Elisabeth Gerstner, Marc-Andre Weber, Tal Arbel, Brian Avants, Nicholas Ayache, Patricia Buendia, Louis Collins, Nicolas Cordier, Jason Corso, Antonio Criminisi, Tilak Das, Hervé Delingette, Cagatay Demiralp, Christopher Durst, Michel Dojat, Senan Doyle, Joana Festa, Florence Forbes, Ezequiel Geremia, Ben Glocker, Polina Golland, Xiaotao Guo, Andac Hamamci, Khan Iftekharuddin, Raj Jena, Nigel John, Ender Konukoglu, Danial Lashkari, Jose Antonio Mariz, Raphael Meier, Sergio Pereira, Doina Precup, S. J. Price, Tammy Riklin-Raviv, Syed Reza, Michael Ryan, Lawrence Schwartz, Hoo-Chang Shin, Jamie Shotton, Carlos Silva, Nuno Sousa, Nagesh Subbanna, Gabor Szekely, Thomas Taylor, Owen Thomas, Nicholas Tustison, Gozde Unal, Flor Vasseur, Max Wintermark, Dong Hye Ye, Liang Zhao, Binsheng Zhao, Darko Zikic, Marcel Prastawa, Mauricio Reyes, and Koen Van Leemput. The Multimodal Brain Tumor Image Segmentation Benchmark (BRATS). *IEEE Transactions on Medical Imaging*, page 33, 2014.
- [10] Samineh Mesbah, Ahmed Shalaby, Sean Stills, Ahmed Soliman, Andrea Willhite, Susan Harkema, Enrico Rejc, and Ayman El-baz. A novel automatic segmentation method to quantify the effects of spinal cord injury on human thigh muscles and adipose tissue. In Maxime Descoteaux, Lena Maier-Hein, Alfred Franz, Pierre Jannin, D. Louis Collins, and Simon Duchesne, editors, *Medical Image Computing and Computer-Assisted Intervention - MICCAI 2017*, pages 703–711, Cham, 2017. Springer International Publishing.
- [11] Fausto Milletari, Nassir Navab, and Seyed-Ahmad Ahmadi. V-net: Fully convolutional neural networks for volumetric medical image segmentation. In *3D Vision (3DV), 2016 Fourth International Conference on*, pages 565–571. IEEE, 2016.
- [12] Haocheng Shen, Ruixuan Wang, Jianguo Zhang, and Stephen J. McKenna. Boundary-aware fully convolutional network for brain tumor segmentation. In Maxime Descoteaux, Lena Maier-Hein, Alfred Franz, Pierre Jannin,

D. Louis Collins, and Simon Duchesne, editors, *Medical Image Computing and Computer-Assisted Intervention - MICCAI 2017*, pages 433–441, Cham, 2017. Springer International Publishing.

- [13] Shuai Zheng, Sadeep Jayasumana, Bernardino Romera-Paredes, Vibhav Vineet, Zhizhong Su, Dalong Du, Chang Huang, and Philip H. S. Torr. Conditional random fields as recurrent neural networks. In *Proceedings of the 2015 IEEE International Conference on Computer Vision (ICCV)*, ICCV '15, pages 1529–1537, Washington, DC, USA, 2015. IEEE Computer Society.